# Supporting Information

## Interfacial-assembly engineering of asymmetric magnetic-mesoporous organosilica nanocomposites with tunable nanoarchitecture

Yangyi Sun[ab1], Yue Wu[ab], Chengyu Zhang[ab], Mengyao He[ab], Dongming Qi[ab2]

[a]*Zhejiang Provincial Engineering Research Center for Green and Low-carbon Dyeing & Finishing, Zhejiang Sci-Tech University, Hangzhou 310018, China.* [b]*Key Laboratory of Advanced Textile Materials and Manufacturing Technology and Engineering Research Center for Eco-Dyeing & Finishing of Textiles, Ministry of Education, Zhejiang Sci-Tech University, Hangzhou 310018, China.*

Corresponding author, email: yangyisun@zstu.edu.cn, dongmingqi@zstu.edu.cn

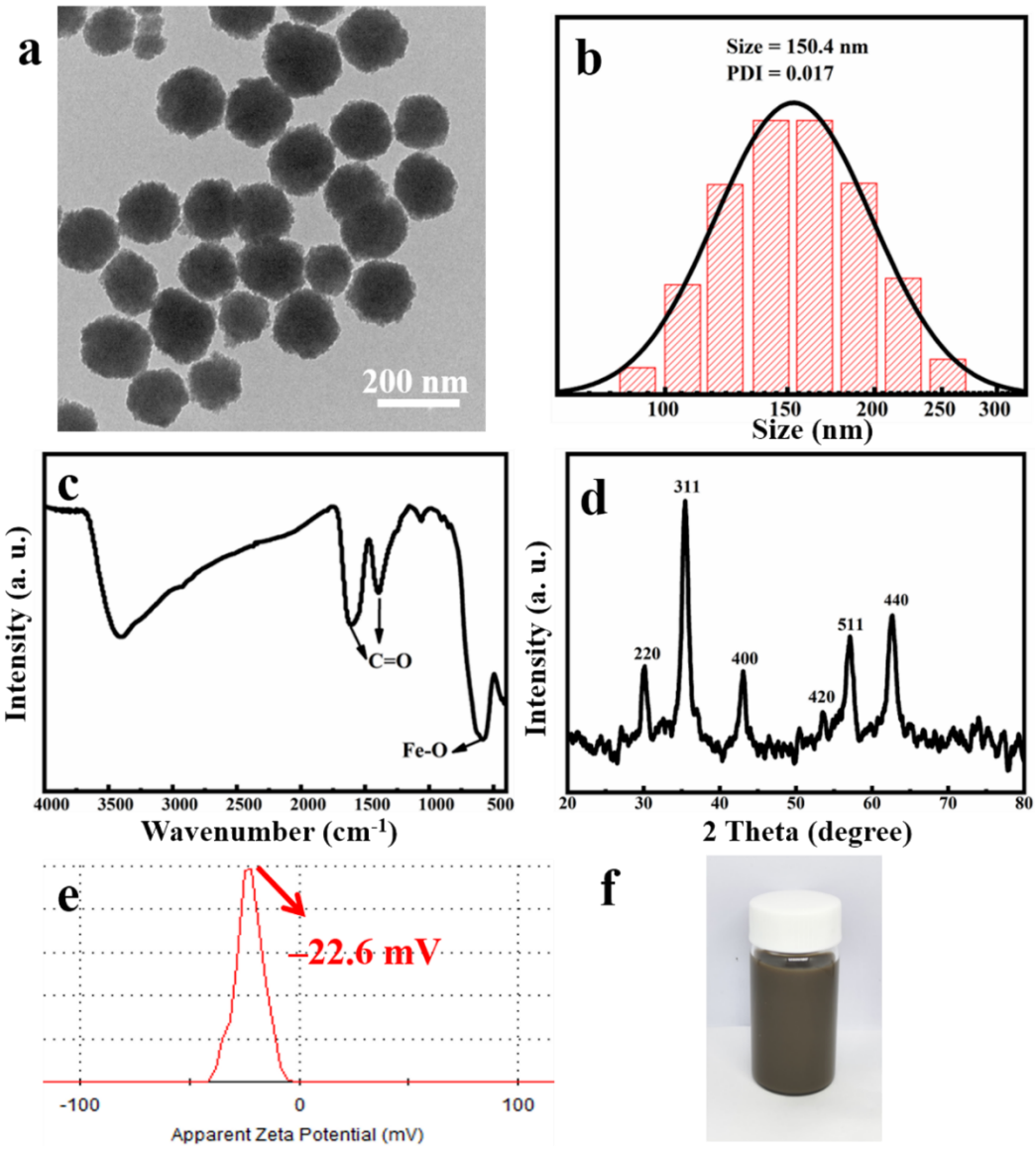


**Figure S1.** (a) TEM image; (b) DLS; (c) FT-IR spectrum; (d) XRD pattern; (e) zeta potential; (f) water dispersion of the $Fe_3O_4$ NPs.

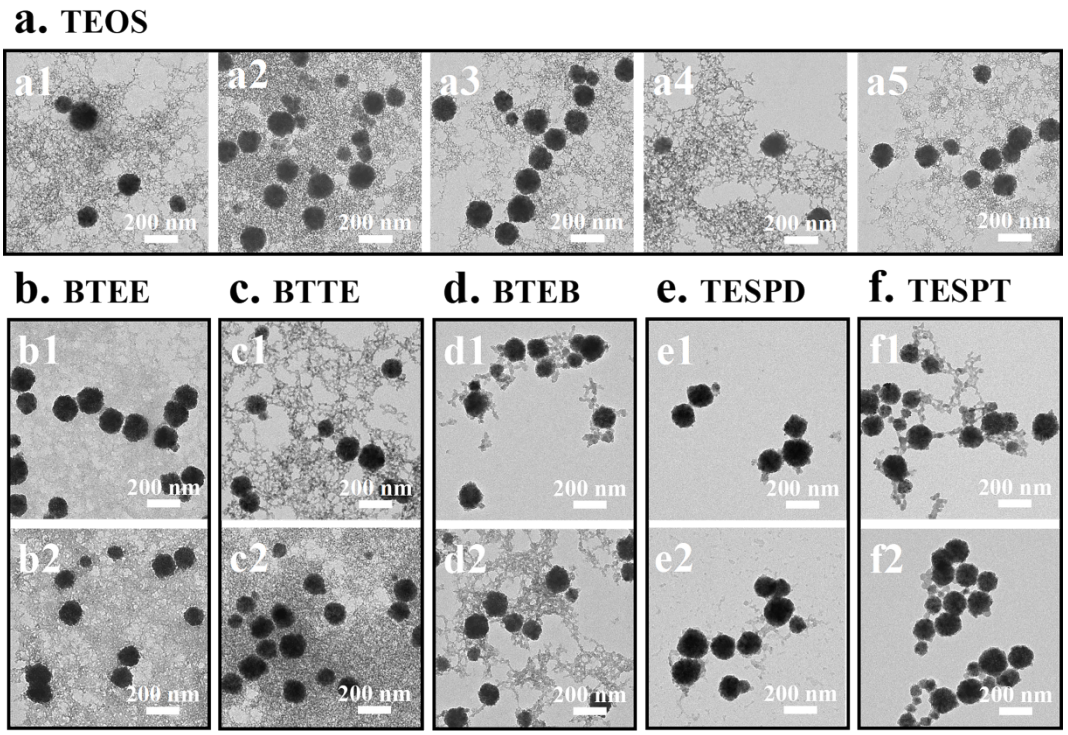


**Figure S2.** TEM images of the NCPs obtained with different silanes without the addition of CTAB: (a) TEOS (a1: 40 ℃, 120 μL, 1.0 mL $NH_3 \cdot H_2O$; a2: 40 ℃, 240 μL, 1.0 mL $NH_3 \cdot H_2O$; a3: 30 ℃, 120 μL, 1.0 mL $NH_3 \cdot H_2O$; a4: 20 ℃, 120 μL, 1.0 mL $NH_3 \cdot H_2O$; a5: 20 ℃, 120 μL, 0.5 mL $NH_3 \cdot H_2O$), (b) BTEE (b1: 120 μL; b2: 240 μL), (c) BTTE (c1: 120 μL; c2: 240 μL), (d) BTEB (d1: 120 μL; d2: 240 μL), (e) TESPD (e1: 120 μL; e2: 240 μL), (f) TESPT (f1: 120 μL; f2: 240 μL). It could be seen that silanes TEOS, BTEE, BTEE, BTEB, TESPD, and TESPT can't nucleate on the surface of $Fe_3O_4$ seeds, evening tunning their reaction kinetics, only the flocculent products of silane are formed around the $Fe_3O_4$ seeds. Even with the use of relatively hydrophilic silane TEOS, no matter whether it accelerates or slows down the reaction kinetics from tuning the amount of TEOS (Figure S2a1-a2), the reaction temperature (Figure S2a2-a4), or the amount of $NH_3 \cdot H_2O$ (Figure S2a4-a5), TEOS could not heterogeneous nucleate and growth on the surface of $Fe_3O_4$ seeds.

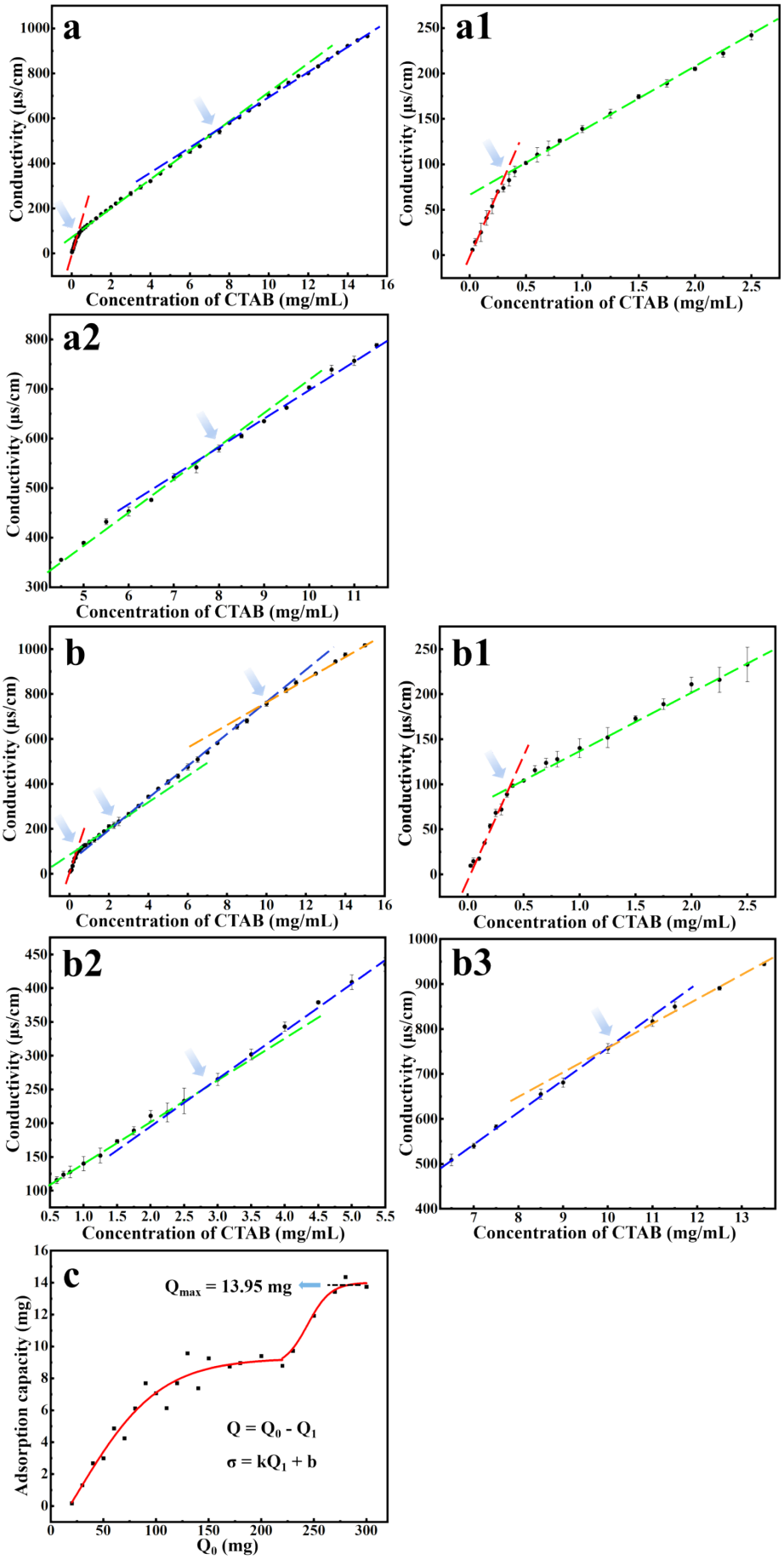
a
Conductivity (μs/cm)
Concentration of CTAB (mg/mL)
a1
Conductivity (μs/cm)
Concentration of CTAB (mg/mL)
a2
Conductivity (μs/cm)
Concentration of CTAB (mg/mL)
b
Conductivity (μs/cm)
Concentration of CTAB (mg/mL)
b1
Conductivity (μs/cm)
Concentration of CTAB (mg/mL)
b2
Conductivity (μs/cm)
Concentration of CTAB (mg/mL)
b3
Conductivity (μs/cm)
Concentration of CTAB (mg/mL)
c
Qmax = 13.95 mg
Q = Q0 - Q1
σ = kQ1 + b
Adsorption capacity (mg)
Q0 (mg)

**Figure S3.** (a) Conductivity versus CTAB concentration in aqueous solution (a1–a2: Local amplification near the inflection points.) and (b) that in the aqueous dispersion of $Fe_3O_4$ seeds (b1–b3: Local amplification near the inflection points.). (c) The adsorption capacity of CTAB on $Fe_3O_4$ seeds. As the conductivity change can be used to determine the critical micelle concentration (CMC) of the CTAB surfactant in solution[1-3] and in the $Fe_3O_4$ solution.[4] The curves of the conductivity against different concentrations of CTAB were measured. As shown in **Figure S3a**, two inflection points appeared in the curve: 0.341 and 7.515 mg/mL (equivalent to 6.82 and 150.3 mg CTAB in 20 mL solution). These values are just the first CMC and second CMC values of pure CTAB solution as the literature reported by other methods.[5, 6] These indicated two CMC values of pure CTAB solution. The first CMC at 0.341 mg/mL is attributed to the formation of spherical CTAB micelles in the aqueous solution, and the second CMC at 7.515 mg/mL belongs to rod-like CTAB micelles formed in the aqueous solution.[2, 7] In an aqueous solution of $Fe_3O_4$-CTAB, as shown in **Figure S3b,** there were three infection points in the curve: 0.406, 2.936, and 10.105 mg/mL (equivalent to 8.12, 58.72, and 202.1 mg of CTAB in 20 mL solution system). The adsorption capacity of CTAB on $Fe_3O_4$ seeds with different amounts of CTAB was shown in **Figure S3c**. When the amount of CTAB is below 200 mg, the adsorption of CTAB on $Fe_3O_4$ seeds increases and is then kept unchanged to reach an adsorption capacity of about 8 mg. When the amount of CTAB is larger than 200 mg, the adsorption capacity is continued to increase and then reaches another adsorption capacity of about 13.95 mg. The changing pattern of adsorption behavior of CTAB on $Fe_3O_4$ seeds is consistent with the change of the zeta potential curve. Thus, we could speculate that the zeta potential curve of $Fe_3O_4$-CTAB would reflect the adsorption behavior of CTAB on $Fe_3O_4$ seeds and the distribution of CTAB in an aqueous solution.

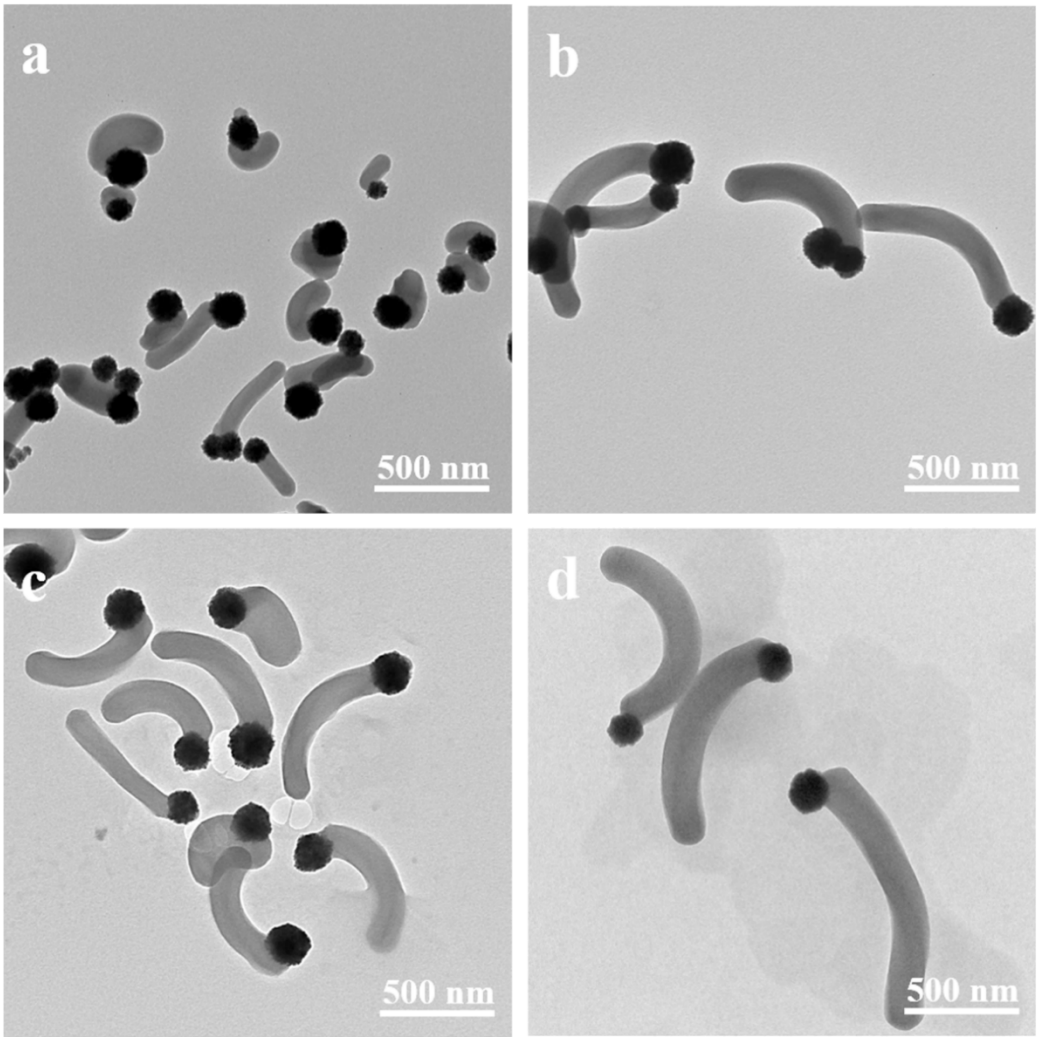


**Figure S4.** TEM images of the $Fe_3O_4$-$SiO_2$ NCPs obtained under 150 mg CTAB and 1.0 mL $NH_3 \cdot H_2O$ with different amounts of TEOS: (a) 100 μL, (b) 120 μL, (c) 150 μL, (d) 180 μL.

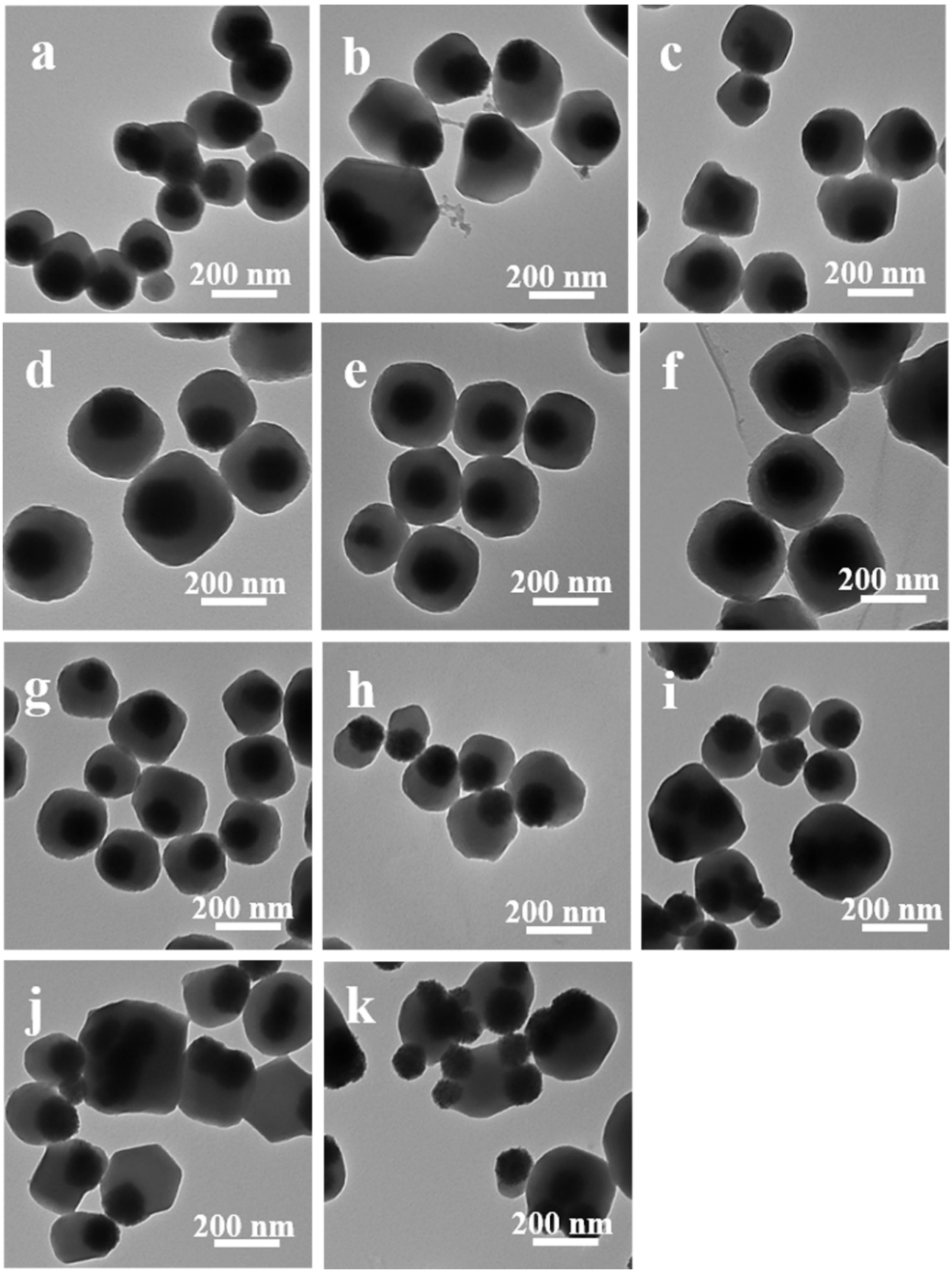


**Figure S5.** TEM images of $Fe_3O_4$-o$SiO_2$ NCPs obtained using 120 μL BTEE: (a-f) with different amounts of CTAB: (a) 10 mg, (b) 30 mg, (c) 50 mg, (d) 75 mg, (e) 100 mg, (f) 150 mg, (g-h) with different amounts of $NH_3 \cdot H_2O$: (g) 0.5 mL, (h) 1.0 mL, (i) 1.5 mL, (j) 2.0 mL, (k) 3.0 mL. It can be seen that the morphology of $Fe_3O_4$-o$SiO_2$ NCPs is eccentric, and core-shell structure.

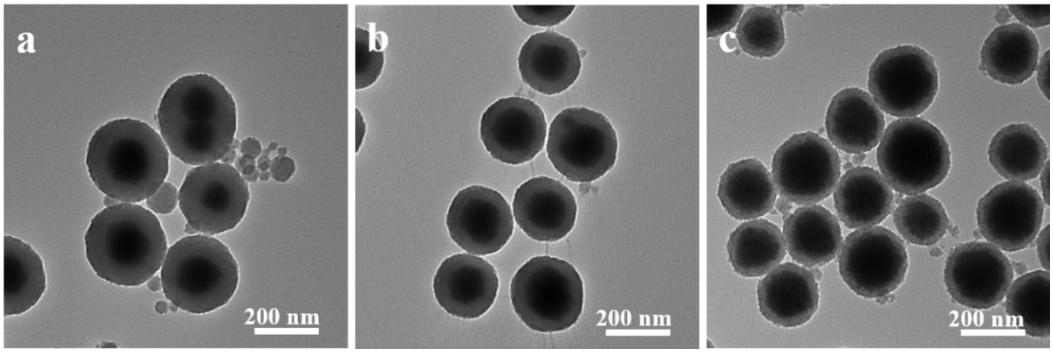


**Figure S6.** TEM images of $Fe_3O_4$-o$SiO_2$ NCPs obtained using 120 μL BTEB with different amount of CTAB: (a) 50 mg, (b) 100 mg, (d) 150 mg.

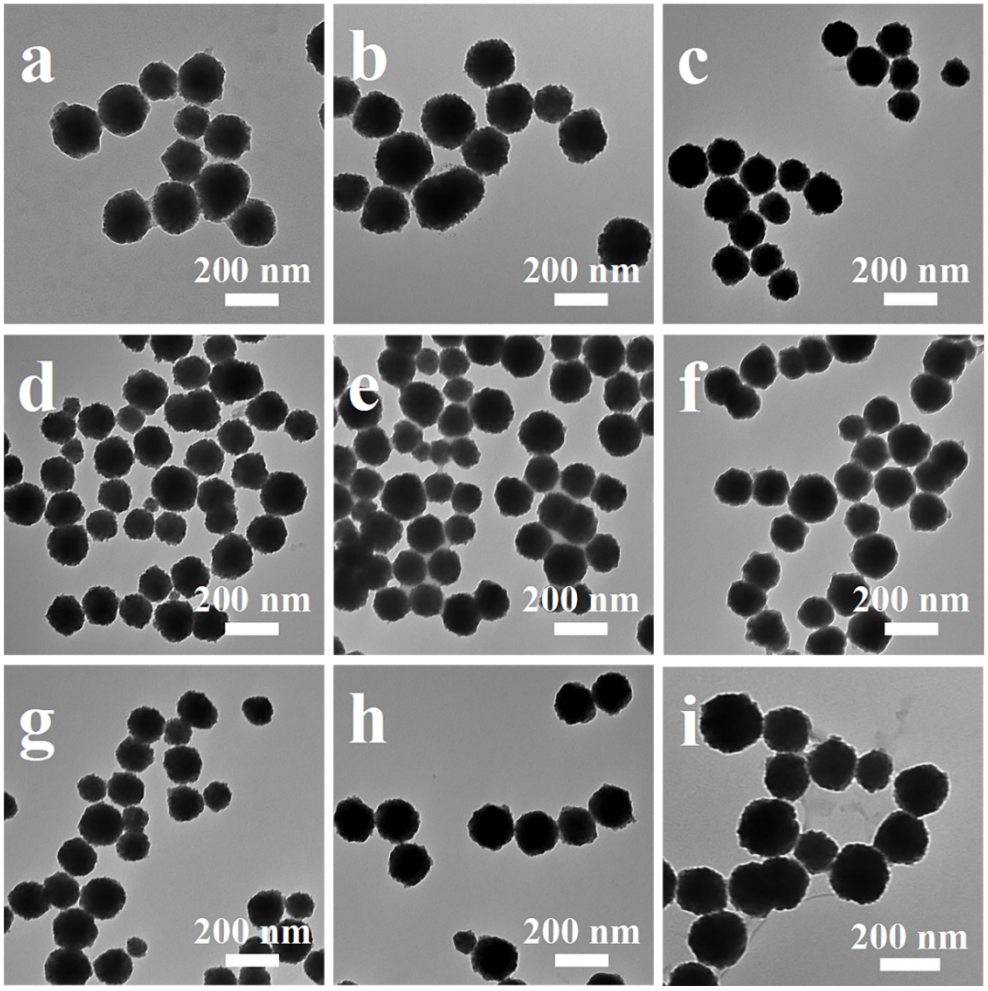


**Figure S7.** TEM images of the NCPs obtained with different silane under different reaction kinetic conditions: (a) 40 ℃, 150 mg CTAB, 120 μL TESPD; (b) 40 ℃, 250 mg CTAB, 120 μL TESPD; (c) 40 ℃, 500 mg CTAB, 120 μL TESPD; (d) 40 ℃, 150 mg CTAB, 120 μL TESPD, 18 mL of water and 2 mL of ethanol; (e) 40 ℃, 150 mg CTAB, 120 μL TESPD, 16 mL of water and 4 mL of ethanol; (f) 40 ℃, 150 mg

CTAB, 120 μL TESPD, 14 mL of water and 6 mL of ethanol; (g) 60 ℃, 150 mg CTAB, 120 μL TESPD; (h) 80 ℃, 150 mg CTAB, 120 μL TESPD; (i) 40 ℃, 250 mg CTAB, 120 μL TESPT. It could be seen that for the silane TESPD, increasing the amount of CTAB (**Figure S7a-c**), tuning the ratio of water and ethanol (**Figure S7d-f**, increasing the reaction temperature (**Figure S7g-h**), the TESPD can't nucleate on the surface of $Fe_3O_4$ seeds.

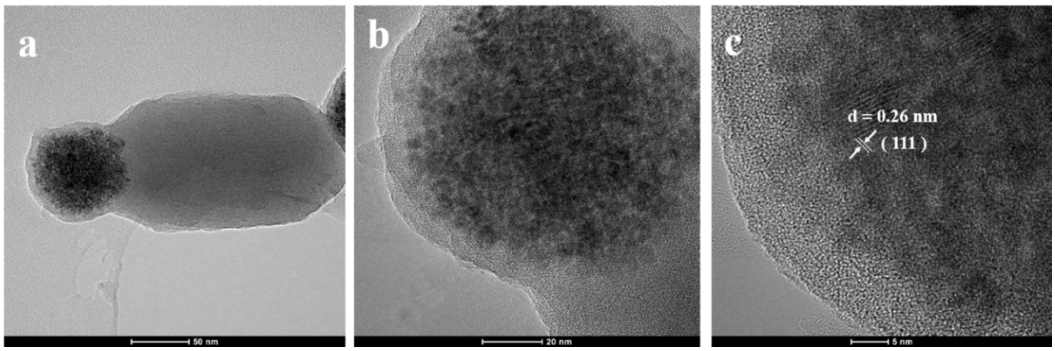


**Figure S8.** TEM image and HRTEM images of asymmetric $Fe_3O_4$-o$SiO_2$ NCPs. The HRTEM image shows the crystal structure of the $Fe_3O_4$ seed.

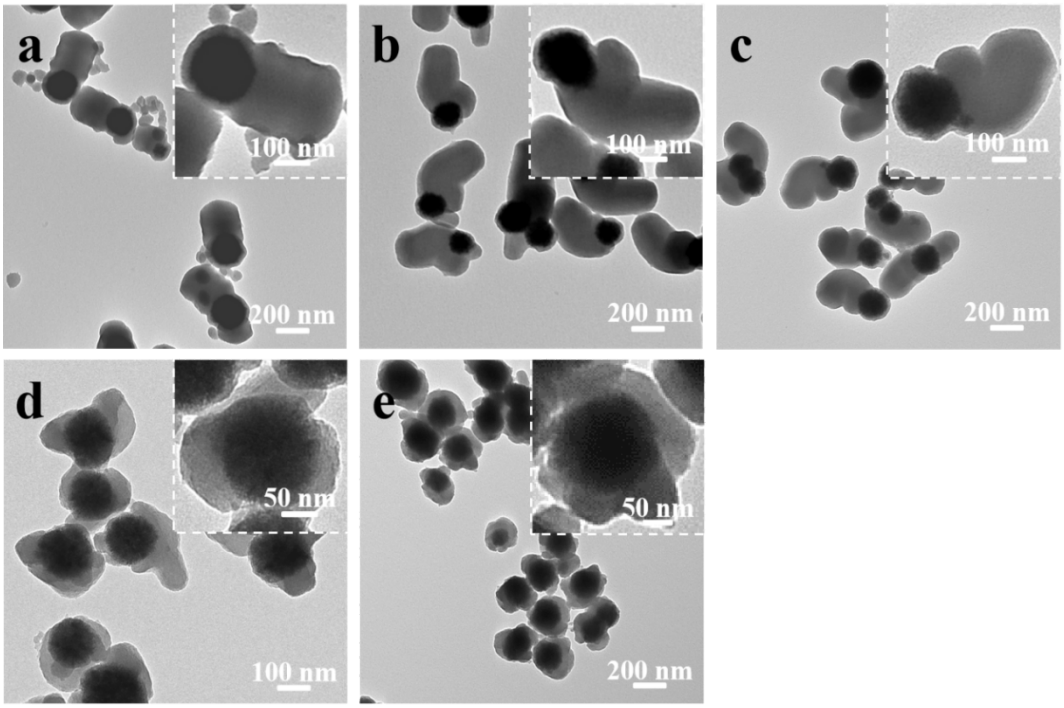


**Figure S9.** TEM images of $Fe_3O_4$-o$SiO_2$ NCPs obtained with different amounts of CTAB: (a) 25 mg; (b) 150 mg; (c) 200 mg; (d) 230 mg; (e) 300 mg.

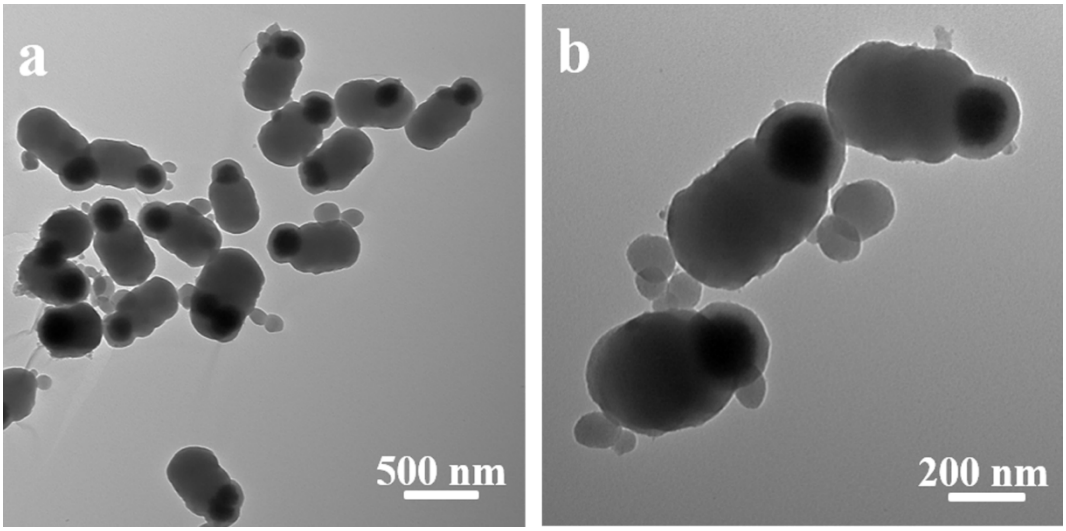


**Figure S10.** TEM images of asymmetric $Fe_3O_4$-o$SiO_2$ NPs obtained with 150 μL BTTE.

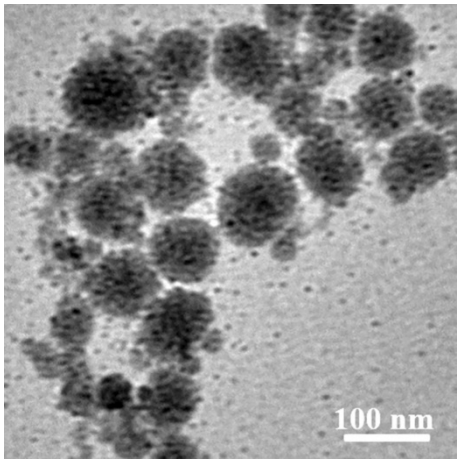


**Figure S11.** TEM image of the supernatant obtained after separating the $Fe_3O_4$-o$SiO_2$ NCPs by an external magnetic field with the temperature of the reaction at 50 °C.

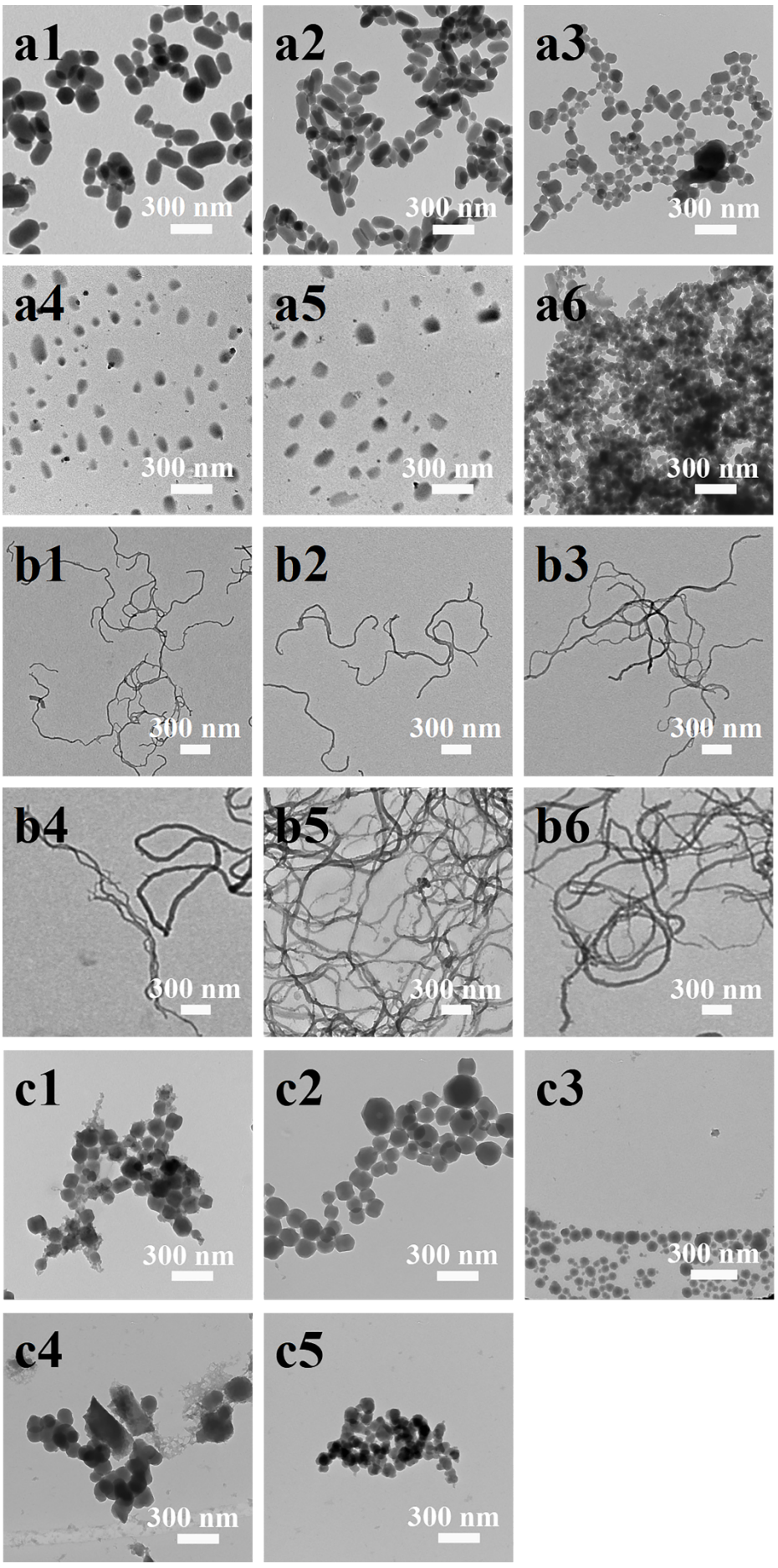
a1
300 nm
a2
300 nm
a3
300 nm
a4
300 nm
a5
300 nm
a6
300 nm
b1
300 nm
b2
300 nm
b3
300 nm
b4
300 nm
b5
300 nm
b6
300 nm
c1
300 nm
c2
300 nm
c3
300 nm
c4
300 nm
c5
300 nm

**Figure S12.** TEM images of $SiO_2$ obtained with different amounts of (a) CTAB: (a1) 25 mg; (a2) 50 mg; (a3) 100 mg; (a4) 200 mg; (a5) 250 mg; (a6) 300 mg, (b) CTATos: (b1) 50 mg; (b2) 100 mg; (b3) 150 mg; (b4) 200 mg; (b5) 250 mg; (b6) 300 mg and (c) CTAC: (c1) 30 mg; (c2) 50 mg; (c3) 200 mg; (c4) 250 mg; (c5) 300 mg.

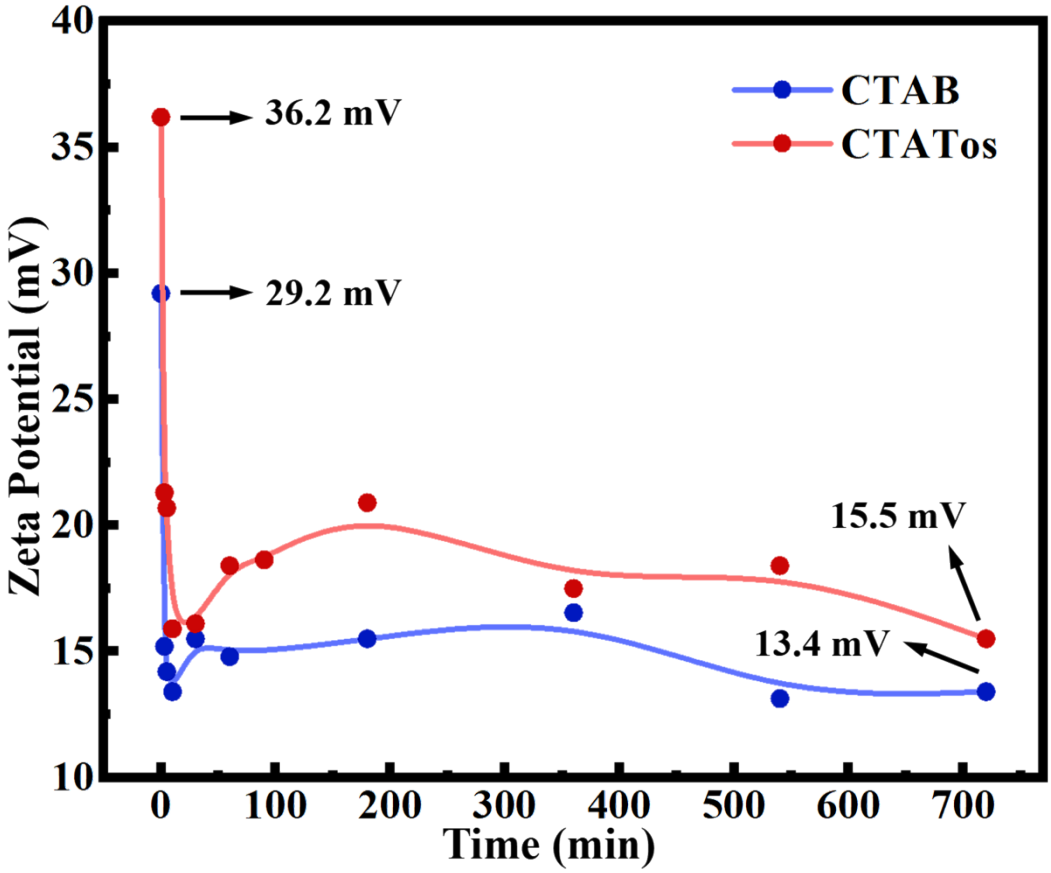


**Figure S13.** Time-dependent surface charge of asymmetric $Fe_3O_4$-o$SiO_2$ NCPs obtained using surfactants CTAB and CTATos.

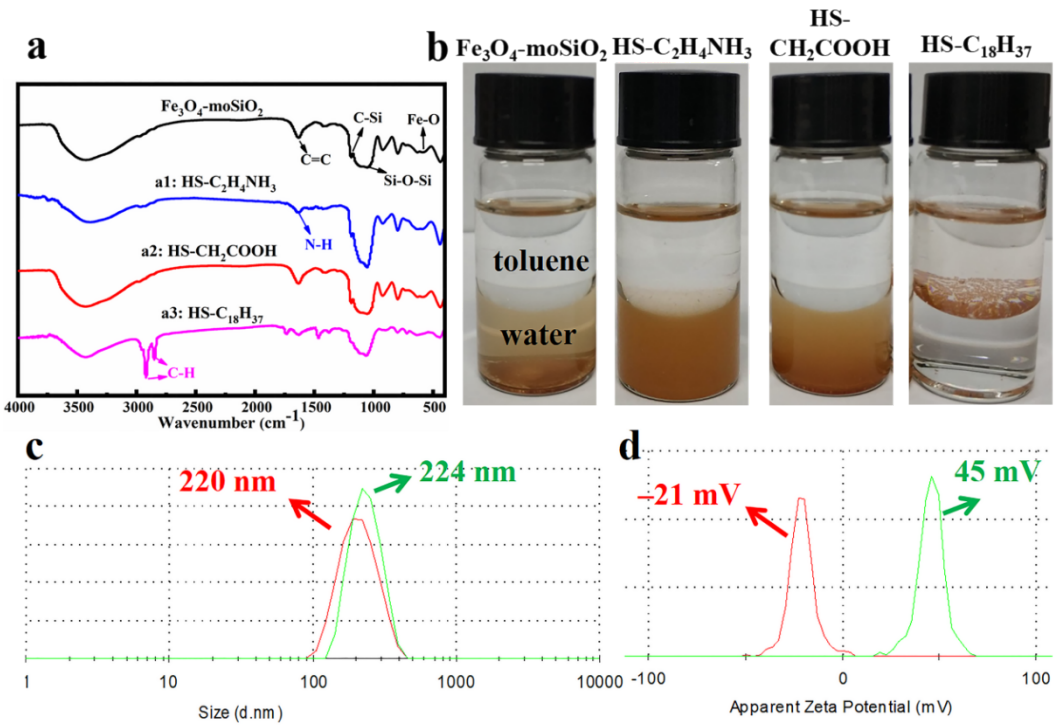


**Figure S14.** (a) FT-IR spectrums of the asymmetric $Fe_3O_4$-o$SiO_2$ and asymmetric $Fe_3O_4$-o$SiO_2$ modified with HS-$C_2H_4NH_3$, HS-$CH_2COOH$, HS-$C_{18}H_{37}$; (b) Scatter photographs of the NCPs dispersed in water/toluene. (c-d) Zeta potential of $Fe_3O_4$-o$SiO_2$ (Red line) and the $Fe_3O_4$-o$SiO_2$ NCPs obtained after modification of (c) APTES; (d) cysteamine (Green line). After HS-$C_2H_4NH_3$ modification, a new absorption peak appeared at 1563 cm$^{-1}$ (**Figure S14a1**), which belongs to $\nu_{N-H}$, and the surface zeta potential increased to +45 mV (**Figure S14d**), indicating the successful grafting of HS-$C_2H_4NH_3$ on the surface of AMMO-NCPs. After modification of HS-$CH_2COOH$, the absorption peak of AMMO-NCPs did not change significantly (**Figure S14a2**), this is mainly because of abundant initial carboxyl groups on the $Fe_3O_4$ NPs surface which affects the display of the characteristic peaks. Meanwhile, after HS-$C_{18}H_{37}$ modification, the peaks that appeared at 2920 and 2849 cm$^{-1}$ belonging to the C-H stretching vibration peak have also appeared (**Figure S14a3**), indicating that $C_{18}H_{37}$ has successfully grafted on the surface of AMMO-NCPs. As shown in **Figure S14b**, when the modified AMMO-NCPs are dispersed in a water/ toluene solution, these modified AMMO-NCPs show obvious tunable hydrophilic/hydrophobic ability. The HS-$C_2H_4NH_3$ and HS-$CH_2COOH$ modified NPs have good solubility in the aqueous phase because of rich hydrophilic groups on the surface. In contrast, the HS-$C_{18}H_{37}$-

modified AMMO-NCPs were dispersed at the water/toluene interface and showed strong hydrophobicity. The thiol-ene click reaction makes the AMMO-NCPs with tunable hydrophilic/hydrophobic properties favorable for further practical applications as abundant SH-enriched species are present commercially.

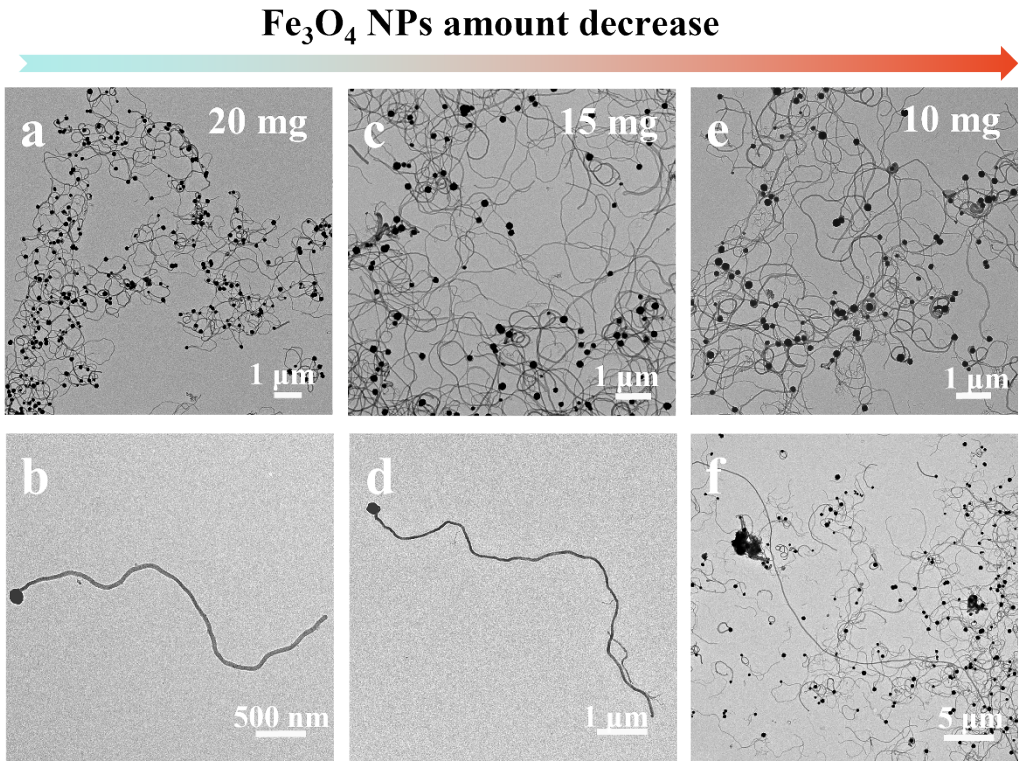


**Figure S15.** TEM images of asymmetric $Fe_3O_4$-o$SiO_2$ NCPs obtained using CTATos with different amounts of $Fe_3O_4$ seed particles: (a) 20 mg; (g) 15 mg; (h) 10 mg.

## References


1. A. W. Ralston, C. W. Hoerr and E. J. Hoffman, *J. Am. Chem. Soc*., 1942, **64**, 97–101.
2. J. F. A. Soltero, J. E. Puig, O. Manero and P. C. Schulz, *Langmuir*, 1995, **11**, 3337–3346.
3. *M. Miura, M. Kodama, Bull. Chem. Soc. Jpn*, 1972, **45**, 428–431.
4. L. Wang and Y. Cao, *Colloids Surf. A Physicochem. Eng. Asp.*, 2018, **553**, 689–694.
5. T. Liu, R. Guo, M. Shen and W. Yu, *Acta Physico-Chimica Sinica*, 1996, **12**, 337–340.
6. N. Li, S. Liu and H. Luo, *Anal. Lett*, 2002, **35**, 1229–1238.
7. Y. Wan and D. Zhao, *Chem. Rev*, 2007, **107**, 2821–2860.